A 103 dBΩ 977 MHz Transimpedance Amplifier for 149 MHz Capacitive MEMS Disk Resonator[1]

Hua Chen[†*], Ke Liu, Zhen Meng[*], and Yuepeng Yan
Smart Sensing Center
Institute of Microelectronics CAS
Beijing, China
mengzhen@ime.ac.cn; chenhua111@mails.ucas.ac.cn

Jinchao Li[†]
Institute of Semiconductors CAS;
University of Chinese Academy of Sciences
Beijing, China

***Abstract*—This paper presents a 103-dBΩ 977-MHz transimpedance amplifier (TIA) for driving VHF-band radial contour-mode MEMS disk resonators. Although the simulation results are given, it is the first time to drive 149 MHz resonators with motional resistance of up to 20 kΩ by using an on-chip circuit. The proposed TIA mainly consists of a regulated-cascode (RGC) amplifier, an inverter-based Cherry-Hooper amplifier, and two buffers. The highlight of the TIA is the resistance-capacitance network, which provides a stable input bias for the Cherry-Hooper amplifier and introduces a leading phase to compensate for the excessive lagging phase of the TIA at 149 MHz. Implemented in the 0.18 µm CMOS process, the TIA occupies a silicon area of 90 µm*40 µm. The simulated gain of the TIA is 103 dBΩ, the -3 dB bandwidth is 977 MHz, and the input-referred current noise is 19.4 pA/√Hz. The MEMS oscillator sets up within 160 µs with an amplitude of 1.37 Vp-p. The simulated phase noise is -114 dBc/Hz at 10 kHz offset and -118 dBc/Hz at 100 kHz offset. The power consumption without buffers is 1.1 mW under supplies of 1.8 V and 1.6 V.**

Keywords—MEMS oscillator; transimpedance amplifier (TIA); wideband; high gain; regulated-cascode (RGC) amplifier

I. INTRODUCTION

MEMS oscillators have become a strong competitor of quartz by the high frequency, integrable, and low-cost advantages. Due to the high frequency and high Q merits, capacitive MEMS resonators draw a lot of research attention. However, the ultrahigh motional resistance prevents them from practical use. Recently, many works have made outstanding achievements on array design [1], process optimization [2], and new mechanism [3], and reduced the motional resistance to a level comparable to piezoelectric resonators and even the quartz. This work endeavors to explore how to design an ultrahigh gain wideband transimpedance amplifier (TIA) from the perspective of the circuit.

Fig. 1 shows the capacitive MEMS disk resonator used in our work and its fitted electrical-model parameters. It works at radial contour mode [4]. At resonance, the resonator can be modeled as an R-L-C series circuit. The resonant frequency is 148.5 MHz with a motional resistance of up to 20 kΩ. To successfully actuate the resonator, the peripheral TIA needs a gain of larger than 94 dBΩ and a bandwidth of 1.49 GHz. Considering the interface parasitic of the TIA and the resonator,

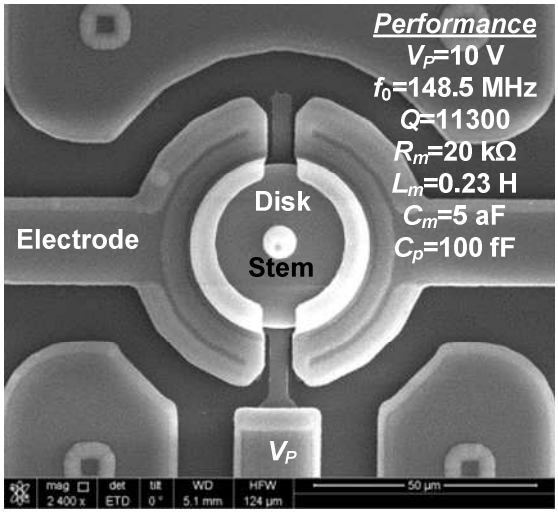

Fig. 1. The 149 MHz radial contour-mode capacitive MEMS disk resonator [4] and its electrical-model parameters.

we set a 0.5 pF capacitor both at the input and output of the TIA. The regulated-cascode (RGC) style is commonly used in the first stage of the TIA to combat the large input capacitance [5, 6]. The popular wideband Cherry-Hooper amplifier [7, 8] is usually employed to obtain high gain. Based on the previous works, this paper proposes an ultrahigh gain wideband TIA by using a resistance-capacitance network, which independently set the input bias of the Cherry-Hooper amplifier and perform a leading phase compensation for the signal at 149 MHz. The TIA is implemented in the 0.18 µm CMOS process, and the simulated gain is 103 dBΩ with a bandwidth of 977 MHz, and input-referred current noise is 19.4 pA/√Hz. Connect the TIA with the resonator to form a closed loop, and the loop gain is 16.8 dB with a phase shift of -5°. The post-simulated phase noise of the MEMS oscillator is -114 dBc/Hz at 10 kHz offset and -118 dBc/Hz at 100 kHz offset.

II. TRANSIMPEDANCE AMPLIFIER DESIGN

The complete schematic of the TIA is shown in Fig. 2. It mainly consists of three stages: an RGC input amplifier with a source-follower; an inverter-based Cherry-Hooper amplifier with a resistance-capacitance network; output buffers.

[1]This work was supported by the National Natural Science Foundation of China (61734007) and the Beijing Natural Science Foundation (4184105). [†]These authors contributed equally.

978-1-6654-3935-0/21/$31.00 ©2021 IEEE

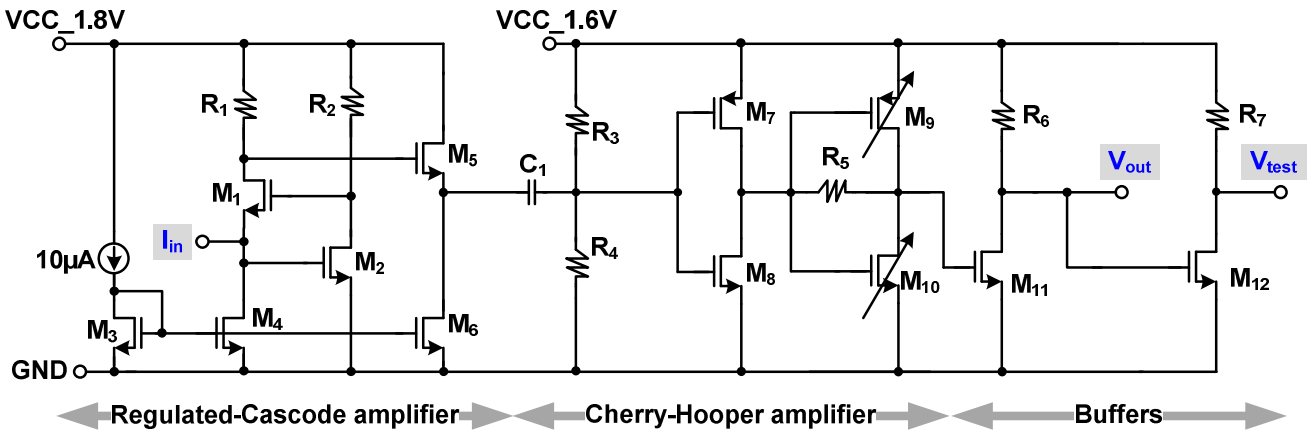

Fig. 2. The proposed TIA with a gain of 103 dBΩ and a bandwidth of 977 MHz for the VHF-band capacitive disk resonator.

The input stage uses the RGC structure to adapt to a large input capacitance, and the common drain amplifier is inserted to isolate the RGC and Cherry-Hooper amplifiers, so that the load resistor of RGC can take a larger value. The resistance-capacitance network made by the C1, R3, and R4, provides inter-stage DC decoupling and leading phase compensation so that the total phase shift of TIA meets the Barkhausen criterion. The Cherry-Hooper adopts an inverter structure to save power and provide significant gain. At resonance, the resonator output voltage is antiphase with its input signal, so an output buffer follows the Cherry-Hooper amplifier. Besides, this buffer also serves as an isolation and amplification function.

The TIA input and output are both loaded by 0.5 pF capacitors to simulate the interface parasitic. For interfacing external measurement instruments, an additional test buffer is also designed on-chip. This test buffer also serves as an output driver for the entire MEMS oscillator. Regarding the high voltage requirement of the input RGC amplifier, the first stage uses a higher power supply of 1.8 V. For saving power consumption, the other circuit share a lower supply of 1.6 V, as illustrated in Fig. 2. For the RGC input stage [6], the input equivalent resistance R_{in}, is:

$$R_{in} = \frac{1}{g_{m1}(1+g_{m2}R_2)} \tag{1}$$

Herein, the g_{m1} and g_{m2} are the transconductance of M1 and M2, respectively. Therefore, increasing the transconductance of the common-gate transistor and raising the gain of the regulated circuit made by M2 and R2 can reduce the input impedance, thereby increasing the bandwidth. The zero frequency that will introduce a peaking in the frequency domain, f_{zero}, is:

$$f_{zero} = \frac{1}{2\pi R_2(C_{gs1}+C_{gs2})} \tag{2}$$

Herein, the C_{gs1} and C_{gs2} are the gate-source capacitance of the M1 and M2, respectively. Increasing the resistance of R2 and reducing the size of the M1 and M2 can push the zero frequency away from the origin. However, maintaining the zero frequency near the upper -3dB bandwidth helps to extend the bandwidth and add some leading phase shift, which can compensate for the lagging phase shift of the RGC input. In addition, maintaining a relatively low peaking is good for the RGC circuit stability.

For the Cherry-Hooper amplifier [7], two identical bias resistors, R3 and R4, are used to provide half of the supply voltage, which is on-chip, stable, and practical. The popular T-shape feedback [7, 8] was simplified by a resistor of R5 for a lower parasitic capacitance. Considering the process deviation, M9 and M10 transistors are tunable to provide a stable output bias of the second stage of the Cherry-Hooper amplifier. On the other hand, the decoupling capacitor of C1 introduces a high-pass characteristic when combining with the bias resistors of R3 and R4. Choose reasonable values of the C1, R3, and R4, so that at the resonant frequency of 148.5 MHz, the leading phase can compensate for the lagging phase of the entire TIA. In addition, small C1 and large R3 and R4 can lower the power consumption of the bias circuit and reduce the size of the on-chip capacitor, which leads to a small parasitic capacitance. The sizing of the TIA is shown in Table I.

III. SIMULATION RESULTS

Based on the 0.18 μm CMOS process, the proposed TIA layout is shown in Fig. 3. The occupied silicon area is 90 μm *40 μm. The simulated frequency response of the TIA is shown in Fig. 3. The TIA shows an ultrahigh gain of 103 dBΩ and a

TABLE I. THE COMPONENT SIZING OF THE PROPOSED TIA.

RGC amplifier		Cherry-Hooper amplifier	
M1	w=10μm, l=0.18μm	C1	c=0.38pF
M2	w=5μm, l=0.18μm	R3=R4	r=10.49kΩ
M3	w=1μm, l=0.18μm	M7	w=9.75μm, l=0.18μm
M4	w=16μm, l=0.18μm	M8	w=3.25μm, l=0.18μm
M5	w=5μm, l=0.18μm	R5	r=10.49kΩ
M6	w=6μm, l=0.18μm	M9	w=3μm, l=0.18μm
R1	r=5.24kΩ	M10	w=1μm, l=0.18μm
R2	r=15.74kΩ		
Buffers			
M11	w=25μm, l=0.18μm	M12	w=15μm, l=0.18μm
R6	r=234Ω	R7	r=67Ω

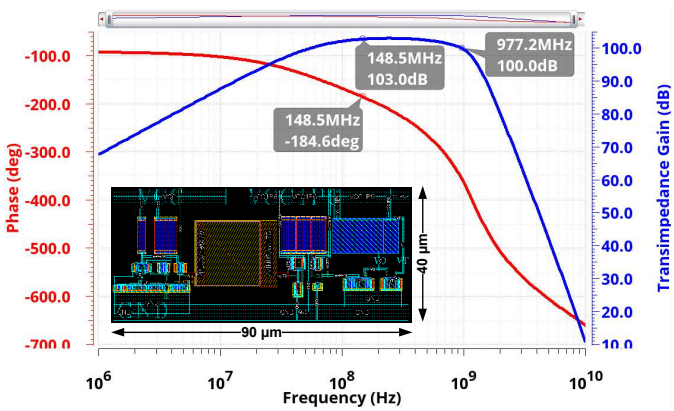

Fig. 3. The simulated TIA gain and phase response. The inset is the TIA layout.

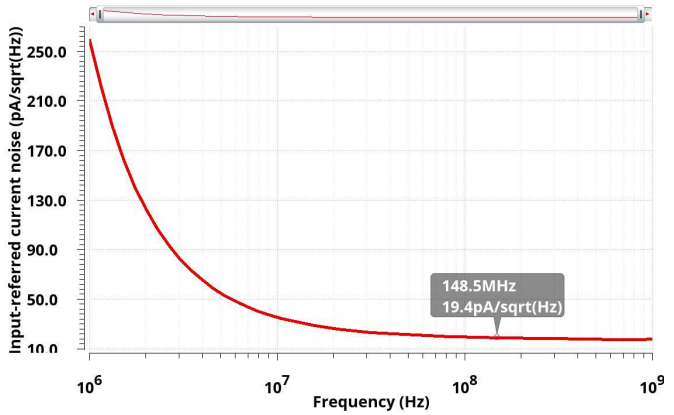

Fig. 4. The simulated input-referred noise current spectrum of the TIA.

wideband of 977 MHz. The TIA gain is high enough to compensate for the motional resistance of the resonator. With the auxiliary aid of the resistance-capacitance network, the total frequency-related phase shift at 148.5 MHz is only -4.6°, which meets the closed-loop positive feedback criterion. In addition, the noise characteristic of the TIA was also simulated, as shown in Fig. 4. The input-referred noise current at the resonant frequency is 19.4 pA/√Hz.

Connect the proposed TIA and the MEMS resonator in a closed loop to simulate the closed-loop stability. The closed-loop frequency response is shown in Fig. 5. The loop gain at the resonant frequency is 16.8 dB, and the total phase shift is -5.2°. The results accord with the frequency response of the presented TIA and meets the design expectations.

Next, do transient simulation and phase noise simulation to check the start-up and phase noise of the proposed MEMS oscillator. The proposed TIA works well with the MEMS resonator, and oscillation sets up within 160 µs with a swing of 1.37 Vp-p as shown in Fig. 6. The highest voltage is about 1.59 V, which is near the supply rail, and the lowest is about 0.22 V. The phase noise at 1 kHz offset (in-band noise) is -93.39 dBc/Hz and the one at 100 kHz offset (out-band noise, also noise floor) is -117.9 dBc/Hz.

The proposed TIA performance and the comparison with other related works are shown in Table II. We can see the

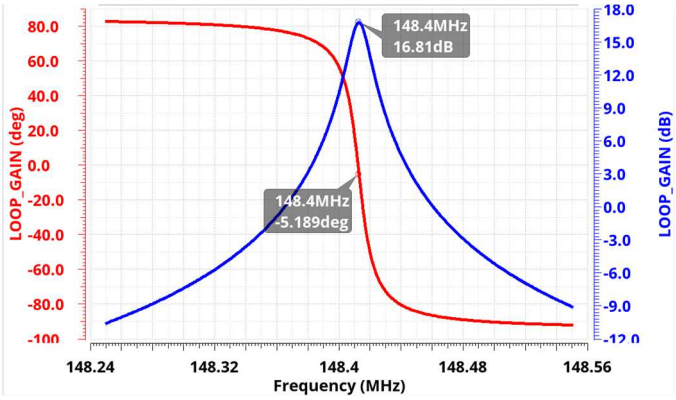

Fig. 5. The simulated loop gain and phase response when connecting the TIA and the resonator in a closed-loop scheme.

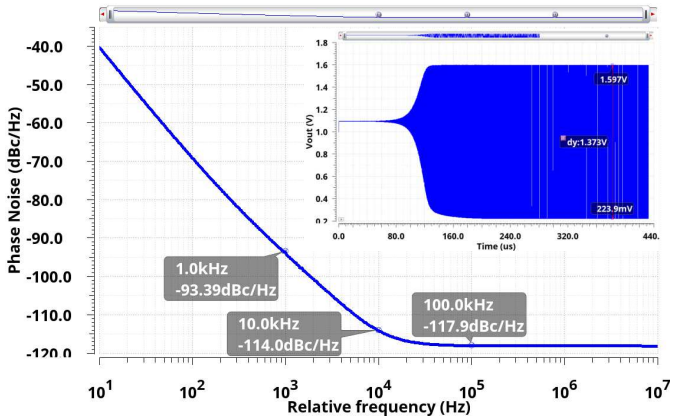

Fig. 6. The simulated MEMS oscillator's start-up process and its phase noise characteristic.

TABLE II. SIMULATED RESULTS OF THE PROPOSED TIA AND THE COMPARISON WITH OTHER SIMILAR WORKS

References	Gain, dBΩ	Bandwidth, MHz	Power, mW
[7][a]	99	280	1.5
[8]	76	2500	7.2
[9]	100	110	8
[10]	101.6	190	37
[11]	86	281	200
[12][a]	82	77	0.05
This work[a]	103	977	1.1

[a.] Simulation results

proposed TIA simultaneously achieves higher gain, larger bandwidth, and lower power consumption. The presented TIA meets the driving requirement of the MEMS disk resonator.

IV. CONCLUSIONS

This paper proposes a 103 dBΩ, 977 MHz, and 1.1 mW transimpedance amplifier implemented in the 0.18 µm CMOS process for the 149 MHz radial contour-mode capacitive MEMS disk resonator. The resistance-capacitance network provides a stable input bias for the Cherry-Hooper amplifier and introduces a leading phase, which compensates for the excessive lagging phase of the total TIA (caused by insufficient -3dB bandwidth). The presented TIA works well with the MEMS resonator, and oscillation builds up within 160 µs with a swing of 1.37 Vp-p. The simulated phase noise at 1 kHz offset is -93.39 dBc/Hz, and

the one at 100 kHz offset is -117.9 dBc/Hz. The subsequent research will focus on the driving circuit of GHz MEMS resonators. This technology provides a design reference for other applications that also require an ultrahigh gain wideband transimpedance amplifier.

ACKNOWLEDGMENT

Hua Chen thanks Quan Yuan, Zeji Chen, Fengxiang Wang, Xiao Kan, and Bohua Peng (Institute of Semiconductor CAS) for MEMS disk resonator characteristic and valuable discussion on the electrical equivalent model of the resonator. Hua Chen and Guoyong Li thanks Xingcheng Zhang and Jixiu Li (Institute of Microelectronics CAS) for help in the EDA software usage.

REFERENCES

[1] Q. Xie, S. Afshar, A. Ozgurluk, and C. T. C. Nguyen, "199-MHz Polysilicon Micromechanical Disk Array-Composite Oscillator," in *2020 Joint Conference of the IEEE International Frequency Control Symposium and International Symposium on Applications of Ferroelectrics (IFCS-ISAF)*, Keystone, CO, USA, 19-23 July 2020, pp. 1-5.

[2] A. Ozgurluk, K. Peleaux, and C. T. C. Nguyen, "Single-Digit-Nanometer Capacitive-Gap Transduced Micromechanical Disk Resonators," in *2020 IEEE 33rd International Conference on Micro Electro Mechanical Systems (MEMS)*, Vancouver, BC, Canada, 18-22 Jan. 2020, pp. 222-225.

[3] Q. Xie and C. T. C. Nguyen, "167-MHz AlN Capacitive-Piezoelectric Oscillator," in *2020 IEEE International Ultrasonics Symposium (IUS)*, Las Vegas, NV, USA 7-11 Sept. 2020, pp. 1-4.

[4] Q. Yuan, W. Luo, H. Zhao, B. Peng, J. Yang, and F. Yang, "Frequency Stability of RF-MEMS Disk Resonators," *IEEE Transactions on Electron Devices,* vol. 62, no. 5, pp. 1603-1608, May 2015.

[5] C. Wei-Zen, C. Ying-Lien, and L. Da-Shin, "A 1.8-V 10-Gb/s fully integrated CMOS optical receiver analog front-end," *IEEE Journal of Solid-State Circuits,* vol. 40, no. 6, pp. 1388-1396, 2005.

[6] S. M. Park and H. J. Yoo, "1.25-Gb/s Regulated Cascode CMOS Transimpedance Amplifier for Gigabit Ethernet Applications," *IEEE Journal of Solid-State Circuits,* vol. 39, no. 1, pp. 112-121, 2004.

[7] M. Li, C. Li, L. Hou, Y. Liu, and S. Li, "A 1.57mW 99dBΩ CMOS transimpedance amplifier for VHF micromechanical reference oscillators," in *2012 IEEE International Symposium on Circuits and Systems (ISCAS)*, Seoul, Korea (South), 20-23 May 2012, pp. 209-212.

[8] H. M. Lavasani, W. Pan, B. Harrington, R. Abdolvand, and F. Ayazi, "A 76 dBΩ 1.7 GHz 0.18 μm CMOS Tunable TIA Using Broadband Current Pre-Amplifier for High Frequency Lateral MEMS Oscillators," *IEEE Journal of Solid-State Circuits,* vol. 46, no. 1, pp. 224-235, 2011.

[9] R. Ma, M. Liu, H. Zheng, and Z. Zhu, "A 66-dB Linear Dynamic Range, 100-dB·Ω Transimpedance Gain TIA With High-Speed PDSH for LiDAR," *IEEE Transactions on Instrumentation and Measurement,* vol. 69, no. 4, pp. 1020-1028, 2020.

[10] P. Wang, M. Ye, X. Xia, X. Zheng, Y. Li, and Y. Zhao, "A Multi-Channel Low-Noise Analog Front End Circuit for Linear LADAR," *IEEE Transactions on Circuits and Systems II: Express Briefs,* vol. 67, no. 7, pp. 1209-1213, 2020.

[11] X. Wang, R. Ma, D. Li, H. Zheng, M. Liu, and Z. Zhu, "A Low Walk Error Analog Front-End Circuit With Intensity Compensation for Direct ToF LiDAR," *IEEE Transactions on Circuits and Systems I: Regular Papers,* vol. 67, no. 12, pp. 4309-4321, 2020.

[12] S. Firouz, E. N. Aghdam, and R. Jafarnejad, "A Low Power, Low Noise, Single-Ended to Differential TIA for Ultrasound Imaging Probes," *IEEE Transactions on Circuits and Systems II: Express Briefs,* vol. 68, no. 2, pp. 607-611, 2021.